Investigation of nickel-impregnated zeolite catalysts for hydrogen/syngas production from the catalytic reforming of waste polyethylene

Dingding Yao[a,b], Haiping Yang[a,*], Hanping Chen[a], Paul T. Williams[b,*]

[a] State Key Laboratory of Coal Combustion, School of Energy and Power Engineering, Huazhong University of Science and Technology, 430074 Wuhan, China
[b] School of Chemical and Process Engineering, University of Leeds, Leeds, LS2 9JT UK

ARTICLE INFO

ABSTRACT

Catalytic steam reforming of waste high density polyethylene for the production of hydrogen/syngas has been investigated using different zeolite supported nickel catalysts in a two-stage pyrolysis-catalytic steam reforming reactor system. Experiments were conducted into the influence of the type of zeolite where Ni/ZSM5-30, Ni/β-zeolite-25 and the Ni/Y-zeolite-30 catalysts were compared in relation to hydrogen and syngas production. Results showed that the Ni/ZSM5-30 catalyst generated the maximum syngas production of 100.72 mmol $g_{plastic}^{-1}$, followed by the Ni/β-zeolite-25 and Ni/Y-zeolite-30 catalyst. In addition, the ZSM-5 supported nickel catalyst showed excellent coke resistance and thermal stability. It was found that the Y type zeolite supported nickel catalyst possessed narrower pores than the other catalysts, which in turn, promoted coke deactivation of the catalyst. Large amounts of filamentous carbons were observed on the surface of the Ni/Y-zeolite-30 catalyst from scanning electron microscope images. In addition, the influence of Si:Al molar ratio for the Ni/ZSM-5 catalysts in relation to hydrogen and syngas yield was investigated. The results indicated that hydrogen production was less affected by the Si:Al ratio than the type of zeolite support. Also, the Ni/ZSM5-30 catalyst was further investigated to determine the influence of different process parameters on hydrogen and syngas yield via different reforming temperatures (650, 750, 850 °C) and steam feeding rate (0, 3, 6 g h^{-1}). It was found that increasing both the temperature and steam feeding rate favoured hydrogen production from the pyrolysis-catalytic reforming of waste polyethylene. The optimum catalytic performance in terms of syngas production was achieved when the steam feeding rate was 6 g h^{-1} and catalyst temperature was 850 °C in the presence of Ni/ZSM5-30 catalyst, with production of 66.09 mmol H$_2$ $g_{plastic}^{-1}$ and 34.63 mmol CO $g_{plastic}^{-1}$.

1. Introduction

Hydrogen is an environmentally-friendly and efficient clean energy with the attraction that its combustion only releases water and energy [1]. Hydrogen production from waste resources such as waste plastics and biomass instead of fossil fuels appears to be more favourable as it overcomes the environmental impact resulting from the over-exploitation of non-renewable resources [2,3]. In addition, considerable amounts of waste plastics are generated each year which a considerable proportion are landfilled, resulting in a waste of resource [4]. Therefore, the production of hydrogen from waste plastics represents an attractive technology for energy recycling in terms of waste management as well as the sustainable ecosystem.

Waste plastics can be thermally converted into hydrogen by pyrolysis-gasification/reforming. A two-stage reaction system was reported by Wu and Williams [5] where pyrolysis of the plastics was followed by catalytic steam reforming of the pyrolysis gases and where the hydrogen production could be optimised by manipulating the process parameters of the two separate processes. The investigation of catalyst promoters and calcination temperature were also carried out to improve the hydrogen production [6]. Barbarias et al. [7] used a two stage spouted-fluidized bed reactor for the continuous production of hydrogen from high density polyethylene in relation to process conditions. Dou et al. [8] optimized hydrogen production from waste plastics by integrating the gasification of the plastics with a sorption-enhanced steam reforming system, where up to 88.4 vol.% of H$_2$ gas concentration was achieved. The feasibility of the two-stage system for hydrogen production was also demonstrated by Czernik et al. [9], where a hydrogen yield of 34 g per 100 g polypropylene was obtained for a 10 h duration test.

Various catalysts have been investigated for hydrogen and syngas production from waste plastics. Ru-based catalysts were prepared by Namioka et al. [10] and Park et al. [11] to catalyse the gasification/reforming of municipal waste plastics, and were found to be effective to

---

compensate for feedstock compositional variations. Currently, nickel is the most commonly used catalyst metal for thermal conversion of hydrocarbons due to its effective activity and lower cost [12]. Mg modified Ni based catalysts have been studied to investigate different operational parameters for hydrogen production and to minimise coke formation during the pyrolysis-catalytic reforming of plastics [13]. Vizcaino et al. [14] suggested the Ni was the phase responsible for enhanced hydrogen production using bimetallic catalysts.

The catalyst support is also important in relation to the activity of the Ni based catalysts. The agglomeration of Ni particles can easily occur in the absence of support, leading to reduction in the catalyst activity [15,16]. Therefore, it is of interest to prepare well-dispersed Ni catalysts using a porous support material. Zeolite catalysts are crystalline, alumina-silicates with an open structure consisting of AlO_4 and SiO_4 tetrahedral crystal structure with a defined pore size and defined microporous structure. Zeolites could provide the porous support material for nickel to aid metal dispersion and enhance catalytic activity for the production of hydrogen-rich syngas. For example, Teh et al. [17] reported that Ni on a ZSM-5 support enhanced the catalytic activity of the catalyst which was attributed to the presence of micro-–mesoporosity and basicity which produced a synergistic effect. The introduction of Ni into the ZSM5 structure has also been suggested to reduce catalyst coke formation by reducing the strong Bronsted acidity of ZSM5, which provide the major active sites for coke formation [18].

The investigations of Ni/zeolite for waste thermal conversions have been investigated by several researchers. Nickel-impregnated ZSM-5 catalysts were prepared and tested by Yung et al. [19] for the upgrading of biomass pyrolysis vapours, where the effects of Ni pre-treatment method and loading were discussed. Karnjanakom et al. [20] reported high catalyst activity and long-term stability of a Ni/MCM-41-EG catalyst for biomass derived tar reforming. Ni based or porous zeolites have also been studied extensively for the catalytic pyrolysis of waste plastics [21–23]. However, there are few detailed researches on hydrogen rich syngas production from waste plastics using different Ni based porous supports such as zeolite. In this paper, different zeolites (ZSM-5, Y-zeolite and β-zeolite) were used as catalyst supports for Ni for the pyrolysis-catalytic steam reforming of waste high density polyethylene (HDPE). The investigation of hydrogen and carbon monoxide yield in relation to zeolite type and Si:Al molar ratio were conducted. In addition, the influence of operational parameters including catalyst reforming temperature and steam feeding rate were also investigated to optimize the syngas production.

2. Materials and methods

2.1. Feedstock and catalyst

High density polyethylene was supplied as recycled waste plastic as 2–3 mm sized pellets by Regain Polymers Limited, Castleford, UK. The ultimate analysis of the plastic feedstock was determined using a Vario Micro Elemental Analyzer, and the elemental content was 84.86 wt.% carbon, 13.64 wt.% hydrogen, 0.98 wt.% oxygen, 0.03 wt.% nitrogen and 0.14 wt.% sulphur. High density polyethylene would not be expected to contain oxygen, nitrogen or sulphur, however, the plastic was a 'real-world' recycled plastic and contained some contamination, possible from other types of plastic. The zeolites used for the pyrolysis-catalytic steam reforming of the waste plastic were purchased from Alfa Aesar and were; ZSM5-30 (ammonium form, Si:Al molar ratio 30, surface area 400 $m^2 g^{-1}$); ZSM5-50 (ammonium form, Si:Al molar ratio 80, surface area 425 $m^2 g^{-1}$); ZSM5-80 (ammonium form, Si:Al ratio 80, surface area 425 $m^2 g^{-1}$); β-zeolite-25 (ammonium form, Si:Al ratio 25, surface area 680 $m^2 g^{-1}$); Y-zeolite-30 (hydrogen from, Si:Al ratio 30, surface area 780 $m^2 g^{-1}$). The ammonium forms of the zeolite support were pre-treated at 450 °C in a muffle furnace under static air for 6 h (with a heating rate of 5 °C min^{-1}) to obtain the protonic form [24].

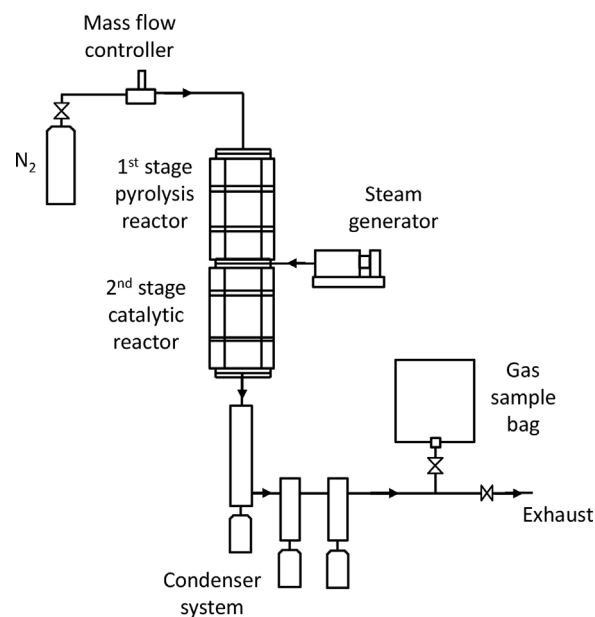Ni introduction into the zeolite support was achieved by an

Fig. 1. Schematic diagram of the reactor system for the pyrolysis-catalytic steam reforming of waste plastic.

impregnation method, 5.50 g $Ni(NO_3)_2 \cdot 6H_2O$ (purchased from Sigma-Aldrich) was completely dissolved into 20 ml ethanol solution, followed by addition of 10 g of the zeolite support so that a Ni loading of 10 wt.% was obtained. The solution was then stirred using a magnetic stirrer at 60 °C to produce a slurry. The precursor slurry was dried overnight and calcined at 500 °C for 3 h (heating rate of 10 °C min^{-1}). The catalyst was then pressed and sieved to obtain particles sizes between 50–212 μm.

2.2. Experimental reactor system and procedure

A schematic diagram of the experimental apparatus for the pyrolysis-catalytic steam reforming of waste HDPE is shown in Fig. 1. The reaction system consisted essentially of a steam feeding system with a water syringe pump, a two-stage stainless steel tube reactor, an inert gas supply system, gaseous product condensing system and gas measurement system. The reactor was externally electrically heated and had two separate heating zones, i.e. first stage plastic pyrolysis reactor of 200 mm height and 40 mm i.d.; second stage catalytic reactor of 300 mm height and 22 mm i.d. The temperatures of the two zones were monitored and controlled separately. In order to explore the effect of different Ni/zeolites on the pyrolysis-catalytic reforming of waste HDPE, two sets of experiment were conducted: the influence of Si:Al ratio of the zeolite support and the influence of zeolite structure type on the yield of hydrogen and syngas. For each experiment, 1 g of waste HDPE and 0.5 g of catalyst were placed in the pyrolysis and reforming stages, respectively. The second catalytic stage was preheated to the catalyst temperature of 850 °C, except where the influence of temperature was investigated, where pre-heating was to 650, 750 or 850 °C. Once the second stage catalyst reactor had reached the desired temperature, the first pyrolysis stage was then heated from room temperature to 500 °C at 40 °C min^{-1} to generate the pyrolysis gases for reforming. In addition, water was injected into the second stage with a flow rate of 6 ml h^{-1} for the catalytic steam reforming process. High purity nitrogen was supplied as inert gas. The condensable liquids were collected in the condensers which were cooled by dry ice, and the non-condensable gases were collected in a 25 l Tedlar™ gas sample bag for gas chromatography (GC) analysis. The total experimental time was around 30 mins. All experiments were repeated to ensure the reliability of the results.

2.3. Product analysis and characterizations

The gaseous products were separated and quantified by packed column gas chromatography (GC). Permanent gases including H_2, O_2, N_2, CO were determined using a Varian 3380 GC/TCD, with a 2 m long and 2 mm diameter column packed with 60–80 mesh molecular sieve. CO_2 was analysed by another Varian 3380 GC/TCD on a 2 m long and 2 mm diameter column packed with HayeSep 60–80 mesh molecular sieve. Both GCs used argon as the carrier gas. Hydrocarbons (C_1 to C_4) were determined on a different Varian 3380 GC/FID using a HayeSep 80–100 mesh molecular sieve column and nitrogen as carrier gas. Gas yield was calculated as mass of gas according to the molar flow of each individual gas and the flow rate of nitrogen. The gas composition of each gas sample was calibrated by standard gases, and showed a standard deviation of less than 0.6 vol.%

The prepared catalysts were characterised using various techniques. The surface area, pore volume and average pore size of the fresh catalysts were calculated from N_2 adsorption and desorption isotherms on an automatic adsorption system (Quantachrome Nova-2200e) operating at 77 K. Samples were initially degassed for 2 h at 200 °C before porosity analysis. The specific surface area was determined by the BET method, and the total pore volume was calculated at a relative pressure P/P_0 of 0.99. The pore distribution was obtained from the desorption isotherms via the BJH method. Powder X-ray diffraction (XRD) patterns of the fresh Ni/zeolites were determined using a Bruker D8 powder X-ray diffractometer, with CuKα radiation at 40 kV and 40 mA. In order to explore the distribution of active sites on the catalysts, the Debye-Scherrer equation (Eq. (1)) was used to obtain the average crystal size from the XRD results. Where, K is a dimensionless shape factor (where K = 0.89 when β is line broadening at half the maximum intensity (FWHM)) and λ is the X-ray wavelength (0.154056 nm). The morphologies of the used catalysts were obtained using a scanning electron microscope (SEM, Hitachi SU8230) operating at 20 kV. A FEI Helios G4 CX DualBeam SEM with precise focused ion beam (FIB) was used to analyse the cross-section of the prepared catalysts, and Ni mapping was obtained with coupled energy dispersive X-ray spectroscopy (EDXS). Before the analysis, the catalyst was coated with platinum in order to protect the sample during the sectioning process. The used Ni/zeolite catalysts were characterized by temperature-programmed oxidation (TPO) with a Shimadzu TGA 50 to determine the properties of carbon deposited on the surface of catalyst. A total of 25 mg of the used catalyst was heated from room temperature to 800 °C in air (100 ml min^{-1}) with a heating rate of 15 °C min^{-1} and a holding time of 10 min at 800 °C. The acidity of the zeolites and Ni impregnated zeolite catalysts were determined by temperature programmed desorption of ammonia (NH_3-TPD) using a BELCAT-M instrument (BEL Japan Inc.) equipped with a thermal conductivity detector (TCD). Each sample (around 50 mg) was initially degassed under 50 ml/min He stream at 550 °C for 2 h. After cooling to 100 °C, the sample was treated with a 5 mol% flow of NH_3 gas (balanced by He) for 1 h, and this was followed by exposure to a He flow for 1 h to remove residual ammonia. Finally, the sample was heated to 700 °C at 10 °C min^{-1} in continuous flow of He, while the concentration of desorbed ammonia was recorded by the TCD.

$$D_{hkl} = \frac{K \cdot \lambda}{\beta \cdot \cos \theta}$$

(1)

3. Results and discussion

3.1. Characterisation of the fresh catalyst

The morphology of the fresh catalysts is shown in Fig. 2. The uniform and porous character of the catalysts can be observed. The Ni/ZSM5-30 and Ni/ZSM5-50 catalysts show rod-like crystals of less than 0.5 μm. For the Ni/ZSM5-80 catalyst, different shapes of crystals and particles with sizes ranging from tens of nanometres to micrometres are seen due to agglomeration. The Ni/β-zeolite-25 catalyst presented uniform spherical crystals of 0.2 μm size while the Ni/Y-zeolite-30 catalyst had a cubic morphology with crystal sizes of around 0.8 μm. Ni particles were well dispersed throughout the catalyst as almost no large Ni particle sizes could be found on the surface, indicating the porous nature and effective role of the zeolite as a support material. The FIB/SEM system was used to provide more information on the structural morphologies and Ni distributions on the cross-section of the catalysts. From Fig. 3(a) and (b), a loose structure can be observed both on the surface and inside of the fresh Ni/ZSM5-30 catalyst, indicating the porous nature of the catalyst. The EDX Ni mapping of the cross-section of the catalyst from Fig. 3(d) shows that Ni was much enriched in the porous structure and was well dispersed on the whole cross-sectional area. Ni was also detected inside the Ni/Y-zeolite-30 catalyst with a good distribution as shown in Fig. 3(e) to (h). Therefore, it is suggested that Ni penetrates into the porous environment of the zeolite, where the catalytic reforming process takes place. In addition, the Ni loading of all the prepared catalysts were checked by SEM-EDX analysis, and the results showed that the obtained Ni loading was 9.97, 11.21, 11.46, 11.08 and 10.87 wt.% for the Ni/ZSM5-30, Ni/ZSM5-50, Ni/ZSM5-80, Ni/β-zeolite-25 and Ni/Y-zeolite-30 catalysts respectively.

The surface areas as well as pore volumes of the Ni/zeolite catalysts are shown in Table 1, and the pore distributions are shown in Fig. 4. The three Ni/ZSM5 catalysts with different Si:Al ratios gave a similar surface area in the range of 225–255 m^2 g^{-1}. The prepared Ni/Y-zeolite-30 catalyst showed a significant higher surface area of 500 m^2 g^{-1}. A maximum total pore volume of 0.657 cm^3 g^{-1} was achieved with Ni/β-zeolite-25 catalyst, which was ascribed to the wide distribution of many mesopores that are illustrated in Fig. 4. From Fig. 4, it can be seen that both micropores and mesopores were present on most of the Ni/zeolite catalysts. The Ni/ZSM5-30 catalyst showed a bimodal pore size distribution, with one peak around 4 nm and another broader peak around 50 nm. In comparison, the Ni/ZSM5-80 catalyst had a single peak of pore size distribution around 4 nm, leading to a total pore volume of 0.099 cm^3 g^{-1}, the lowest of all the catalysts. It suggests that the mesopores were decreased with increasing Si:Al ratio of the catalyst support. The Ni/Y-zeolite-30 catalyst also showed a bimodal distribution of pore size, however, the corresponding pore diameter was much smaller than it of the Ni/ZSM5-30 catalyst.

The XRD spectra for the calcined catalysts are shown in Fig. 5. The diffraction peaks of NiO for all the fresh catalysts were weak and broad, indicating that the active Ni sites were well dispersed on the support and were small, which was also demonstrated by Ni EDX mapping shown in Fig. 2(f). According to the Scherrer equation, the nickel particle size was 15 nm for the Ni/ZSM5-30 catalyst, and increased a little to 30 nm for the Ni/ZSM5-80 catalyst with higher Si:Al ratio. This may due to the decrease of inter-particle pores with increasing Si:Al ratio from the isotherm data and SEM images, suggesting the nickel was less dispersed on the surface for the Ni/ZSM5-80 catalyst compared with the Ni/ZSM5-30 catalyst. However, the nickel crystallite size for β-zeolite and Y-zeolite supported catalysts were difficult to be determined owing to the broadening of the diffraction peak; it also suggests that Ni species were well dispersed on both of these zeolites. In addition, the XRD spectra of the spent Ni/ZSM5-30 catalyst is also shown in Fig. 5. It can be seen that all the NiO compounds in of the fresh catalyst were converted into monotonic Ni, indicating that the nickel oxides of the prepared catalyst after calcination can be reduced into metallic Ni during the pyrolysis-catalytic reforming process without an additional catalyst reduction step. In addition, the used catalysts were also studied by XRD analysis. The results showed that the Ni crystallite sizes were 38, 42, 48, 36 and 25 nm for the Ni/ZSM5-30, Ni/ZSM5-50, Ni/ZSM5-80, Ni/β-zeolite-25 and Ni/Y-zeolite-30 catalysts respectively. It indicated that the active particle size was increased during the experiments, especially for the ZSM5 based Ni catalysts, which may be due to the relatively high catalyst temperature (850 °C) used in this work.
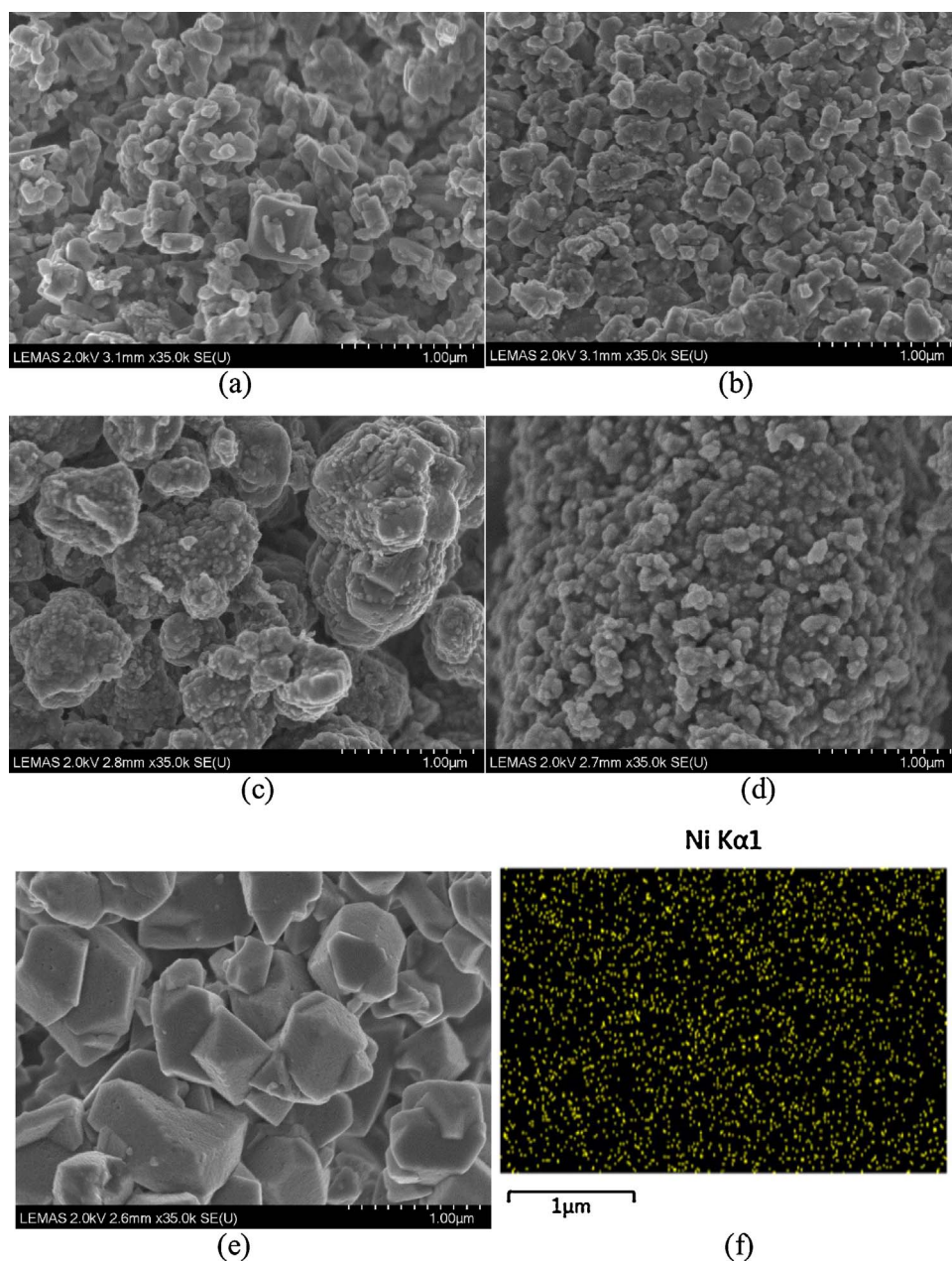
Fig. 2. SEM images of fresh Ni/zeolites catalyst. (a) Ni/ZSM5-30, (b) Ni/ZSM5-50, (c) Ni/ZSM5-80, (d) Ni/β-zeolite-25, (e) Ni/Y-zeolite −30, (f) Ni EDX-mapping of fresh Ni/ZSM5-30.

The acidity of different zeolite and Ni/zeolite samples were investigated by NH_3-TPD analysis, and the results are shown in Fig. 6. Generally, the acid sites can be classified by strength into two types according to the ammonia desorption temperature [25]. Two major desorption peaks at 250 °C and 450 °C were related to weak and strong acid sites, respectively. The TPD profiles of the parent zeolites were overlapped by two desorption peaks. The ZSM5-30 support appeared to be the zeolite with highest acidity for both weak and strong acid sites. The β-zeolite-25 support presented more weak acidity than strong acidity. The Y-zeolite support showed very little weak acidity but a broad strong acidity peak. After impregnation of Ni, the weak acid sites were significantly reduced whereas the strong acid sites were much increased, especially for the Ni/ZSM5-30 catalyst. The increase of the new acid sites at high temperature may be due to the aluminium species derived from the framework dealumination [26], which was also indicated by XRD results. And the additional acid sites were also reported to provide an electron pair acceptor which benefits the catalytic process [24].

3.2. Influence of zeolite type on hydrogen and syngas yield from waste plastic

The influence of different types of Ni-based zeolite catalyst on the hydrogen and syngas production from the pyrolysis-catalytic steam reforming of waste high density polyethylene was investigated at a catalyst temperature of 850 °C and steam feeding rate of 6 g h^{-1}. The different catalysts compared were, Ni/ZSM5-30, Ni/β-zeolite-25 and the Ni/Y-zeolite-30 catalysts. The results of syngas production and gas compositions are shown in Table 2. The calculated mass balance for all the catalytic experiments ranged from 97 to 105 wt.%, indicating the reliability of experiments, and the standard deviations of the hydrogen and carbon monoxide yield for the repeated experiments were also calculated, with an average value of 1.07 and 0.85 mmol g$_{plastic}^{-1}$ respectively. Hydrogen yield and carbon monoxide yield were 55.85 mmol g$_{plastic}^{-1}$ and 31.30 mmol g$_{plastic}^{-1}$ respectively for the non-catalytic experiment, where 0.5 g sand was used in the second stage in place of the catalyst. The parent zeolites after pre-treatment without Ni loading were also used for the pyrolysis-reforming process. ZSM5-30
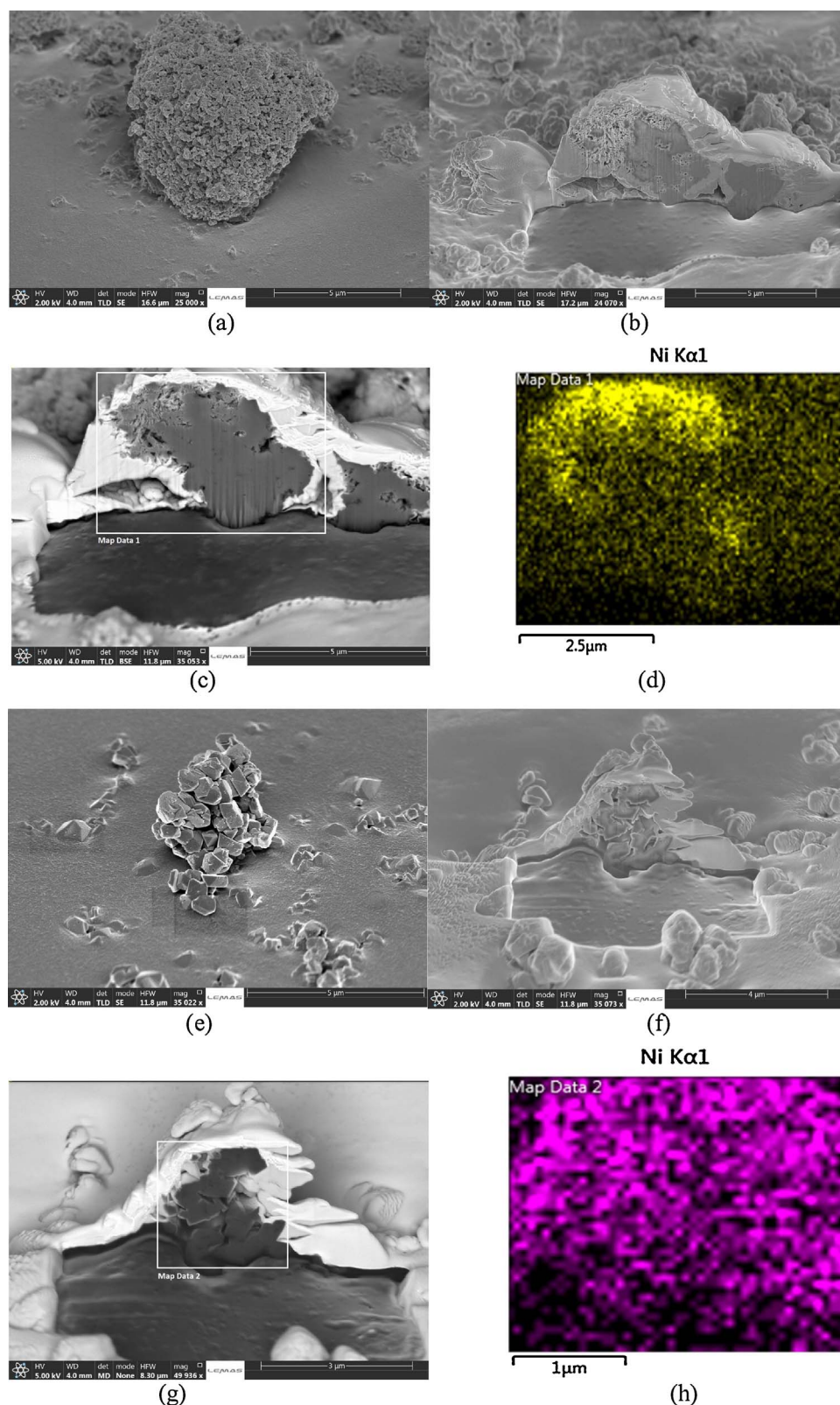
Fig. 3. Cross-section images of fresh catalysts: (a), (b) and (c) are Ni/ZSM5-30 in different magnification; (d) is the EDX Ni mapping of the specified area in image c; (e), (f) and (g) are Ni/Y-zeolite-30; (h) is the EDX Ni mapping of the specified area in image g.

generated higher hydrogen yield of 57.44 mmol H_2 $g_{plastic}^{-1}$ than the other two types of zeolites, which may be due to the large amounts of surface acidity of ZSM5-30 as indicated in Fig. 5. Nevertheless, very little catalytic effect was observed for all the non-impregnated zeolite, as the H_2 yield and CO production were very similar compared with the non-catalytic trial. However, when the reforming conditions such as the temperature or steam feeding rate were changed, the gas yields were influenced significantly (as shown in the following Section, 3.4). It may be concluded that the steam reforming reactions were quite sufficient at this high temperatures (850 °C) with a steam feeding rate of 6 g h^{-1}, and more reactive active catalysts such as Ni rather than the zeolites without Ni were needed to further catalyse this process to produce more hydrogen.

The main gases produced were H_2, CO, CH_4 and CO_2. Both H_2 and

Table 1
The surface area and pore volume of different Ni/zeolite catalysts.

	Si:Al	Surface Area ($m^2 g^{-1}$)	Total pore volume ($cm^3 g^{-1}$)
Ni/ZSM5-30	30	229	0.135
Ni/ZSM5-50	50	244	0.183
Ni/ZSM5-80	80	253	0.099
Ni/β-zeolite-25	25	324	0.657
Ni/Y-zeolite-30	30	500	0.215

CO production were promoted with the introduction of catalyst. The Ni/ZSM5-30 catalyst generated the highest syngas yield of 100.72 mmol $g_{plastic}^{-1}$, with a H_2 yield of 66.09 mmol $g_{plastic}^{-1}$ and a CO yield of 34.63 mmol $g_{plastic}^{-1}$. The syngas production for the Ni catalysts with different zeolite supports decreased in the order of Ni/ZSM5-30 > Ni/β-zeolite-25 > Ni/Y-zeolite-30. Little difference in gas compositions could be found between the different catalysts, and hydrogen and CO content remained around 55 vol.% and 30 vol.% respectively.

The amount and the type of coke deposition on the catalyst after the pyrolysis-catalytic steam reforming was determined by TPO analysis. From Fig. 7, the oxidation of the used catalyst consisted of three stages: the removal of water from 100 to 300 °C, the oxidation of Ni to NiO in the range of 350–500 °C, and coke combustion after 500 °C. The small increase in the weight of used catalyst was due to the oxidation of elemental Ni (derived from the NiO reduction during the experiment). The amount of coke deposition was determined from the weight loss after 500 °C divided by the raw sample weight for the TPO experiment. The results showed that the coke deposited on the catalyst decreased in the order of Ni/Y-zeolite-30 > Ni/β-zeolite-25 > Ni/ZSM5-30. Less than 0.5 wt.% of coke was detected for the Ni/ZSM5-30 catalyst, indicating effective coke resistance during the pyrolysis-catalytic steam reforming process. The TPO results for the reacted Ni/β-zeolite-25 catalyst also showed little weight loss during the oxidation. However, nearly 6 wt.% of coke deposition was found for the Y type zeolite supported Ni catalyst, as indicated by the TPO weight loss between 550–700 °C, where the oxidation mainly occurred at ~600 °C. There are commonly two types of carbon deposited on Ni-based catalysts [27] The oxidation of amorphous carbon or layered carbon occurs at
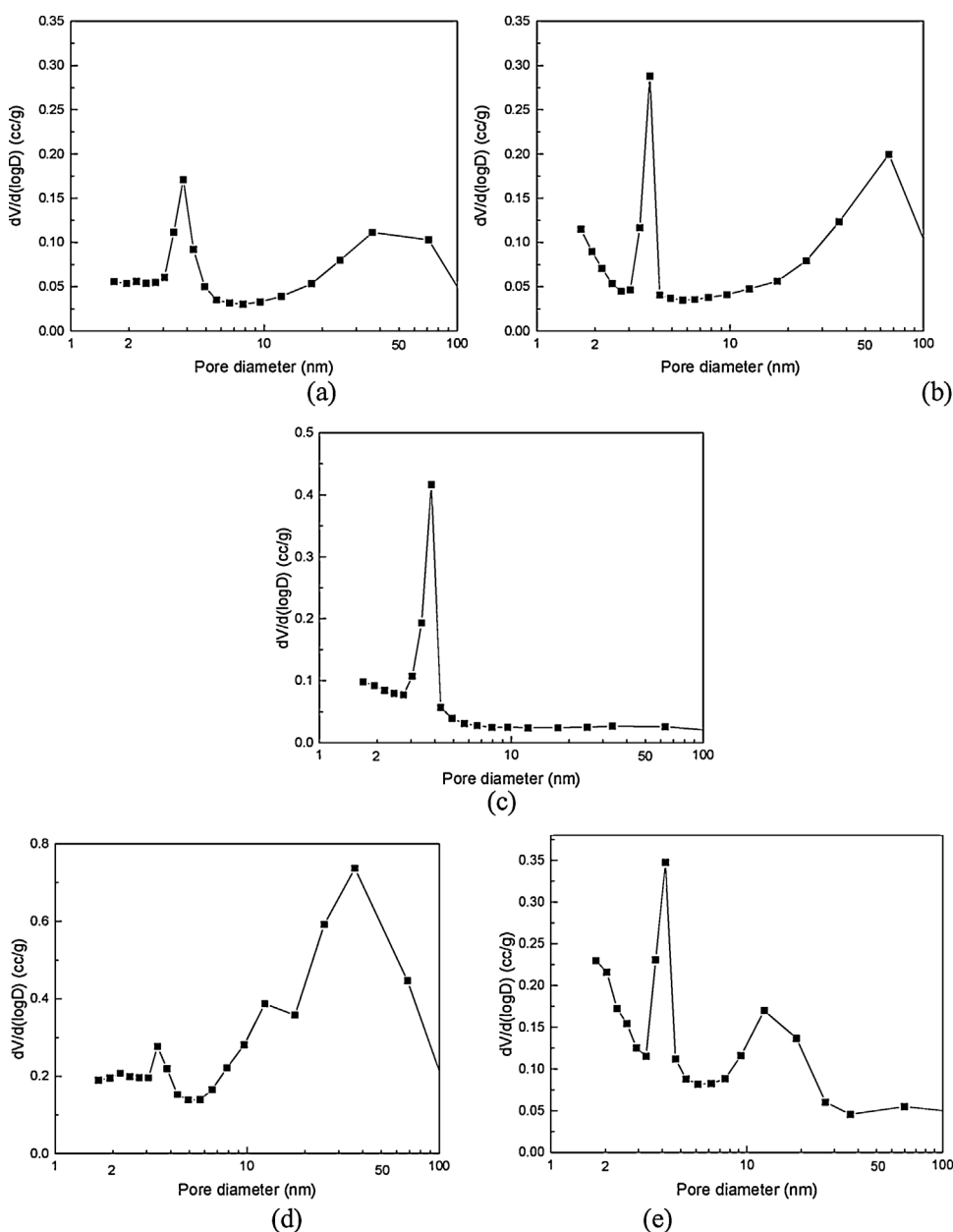

Fig. 4. Pore size distributions of prepared Ni/zeolite catalysts. (a) Ni/ZSM5-30, (b) Ni/ZSM5-50, (c) Ni/ZSM5-80, (d) Ni/β-zeolite-25, (e) Ni/Y-zeolite-30.
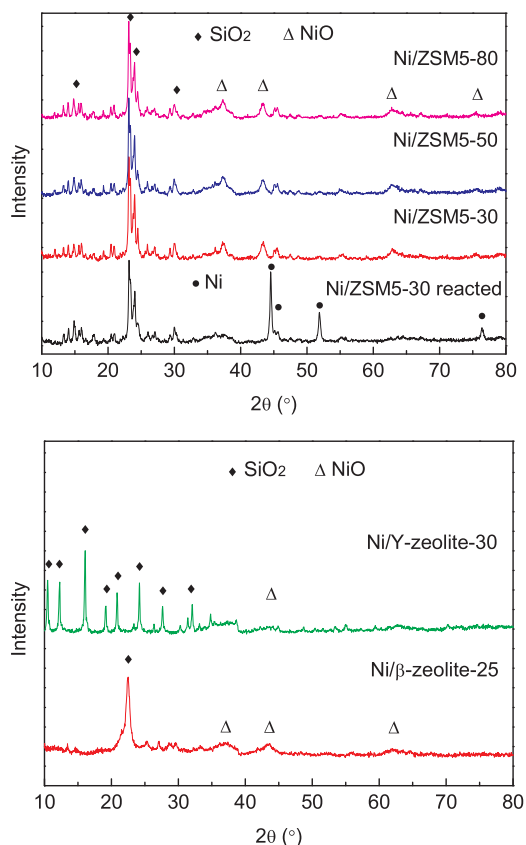
Fig. 5. X-ray diffraction profiles of the fresh and spent Ni/zeolite catalysts.
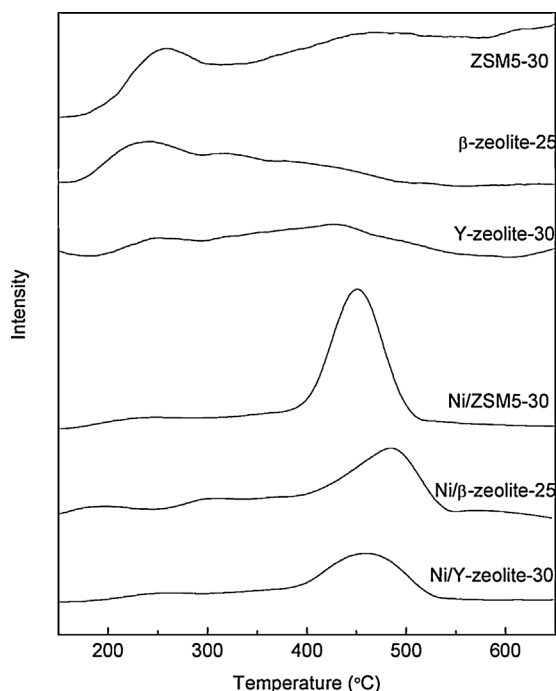

Fig. 6. NH₃-TPD profiles of the parent and impregnated zeolites.

~500 °C, and the oxidation of filamentous carbon is suggested to start from ~600 °C. Therefore, the coke obtained from Ni/Y-30 catalyst in this work was assigned to the filamentous type carbon. Ochoa et al. [28] studied the coke formation and deactivation mechanism of Ni catalysts for the steam reforming of pyrolysis volatiles from waste polyethylene at a catalyst temperature of 700 °C. They reported that the

coke formation evolved initially encapsulating coke by carbon precursors and Ni particles sintering, followed by coke carbonization to form the filamentous coke with graphitic layers. The growth of Ni particles was also observed from the XRD results shown in Fig. 5. However, more coke deposition was observed in this work which was of the filamentous type, which may due to a relatively higher catalyst temperature of 850 °C which accelerates the first step and the carbonization of the coke.

Fig. 8 shows the SEM images of the spent Ni/ZSM5-30, Ni/β-zeolite-25 and the Ni/Y-zeolite-30 catalysts. No coke was detected on the used Ni/ZSM5-30 catalyst, and only few carbon deposits were found for the Ni/β-zeolite-25 catalyst. By comparison, filamentous type carbons could be observed on the Ni/Y-zeolite-30 catalyst, suggesting that the Y type zeolite supported Ni catalyst was more susceptive to coke deposition. The coked deposited on the catalyst may lead to a lowering of the catalytic activity towards the pyrolysis-catalytic reforming of waste plastics. The deposited carbons displayed a uniform diameter of around 50 nm and with length up to few microns. Compared with the freshly prepared Ni/zeolite catalysts shown in Fig. 2, the Ni/ZSM5-30 catalyst retained its structure and morphology after reaction. Ni EDX-mapping of the catalyst shown in Fig. 8(d) and (e) shows well-dispersed nickel sites on the spent Ni/ZSM5-30 catalyst, indicating its good stability during the catalytic process. The results revealed by the SEM morphologies were in good agreement with the TPO results. Wong et al. [26] studied the catalytic cracking of low density polyethylene with Ni catalysts supported by different zeolites, they also found that the catalyst supported by Y type zeolites were more susceptible to coke formation, while ZSM5 supported catalysts showed better performance in inhibiting coke deposition. Coke formation on the surface of zeolites was reported to be a shape-selective process [29]. The cage structure of Y type zeolite provides suitable space for coke formation which leads to the deactivation of the catalyst. However there is no cage-like structure in ZSM5, the inter-crossed connection of the channels and its particular three-dimensional ten-membered ring framework inhibit the formation of condensed-ring aromatics (coke) [30,31]. On the other hand, coke formation may also be influenced by the steric constraint or diffusion limit [32], where a smaller pore size zeolite tends to lead to higher selectivity to coke formation because of the rapid blockage by coke or coke precursors of the pores. From Fig. 4, relatively larger meso-pores (around 40 nm) were mainly produced for the Ni/ZSM5-30 and Ni/β-zeolite-25 catalysts compared with the Ni/Y-zeolite-30 catalyst, therefore, the coke was reduced and the catalytic reactions were promoted because more hydrocarbons could enter inside the pores of the catalysts.

3.3. Influence of zeolite support Si:Al ratio on pyrolysis-reforming of plastic wastes

In this section, Ni-based ZSM5 supported catalysts with different Si:Al ratios from 30 to 80 (designated as ZSM5-30 ZSM5-50 and ZSM5-80) were investigated for their influence on the pyrolysis-catalytic steam reforming of waste plastic. The gas yield and volumetric gas composition and product mass balance are shown in Table 3. The results showed that the Ni/ZSM5-30 catalyst produced the highest shows hydrogen and syngas yield. Both H_2 yield and CO yield slightly decreased with the increase in the Si:Al ratio of the Ni/ZSM5 catalyst. The syngas yield was 100.72 mmol $g_{plastic}^{-1}$ for the Ni/ZSM5-30, which decreased to 91.54 mmol $g_{plastic}^{-1}$ in the presence of the Ni/ZSM5-80 catalyst. The gas yield reached a minimum of 147.58 wt.% when the Si:Al ratio of Ni/ZSM5 was 50. As for the gas composition, there was little difference observed for the volumetric gas concentrations among the different catalysts.

The TPO analyses of the spent Ni/ZSM5 catalysts are show in Fig. 9. The increase in catalyst mass during oxidation was due to the oxidation of monometallic Ni, which was reduced by the reducing gases like H_2 and CO produced during the reforming process which then were

Table 2
Gas production from pyrolysis-reforming of waste polyethylene at 850 °C and steam feeding rate of 6 g/h.

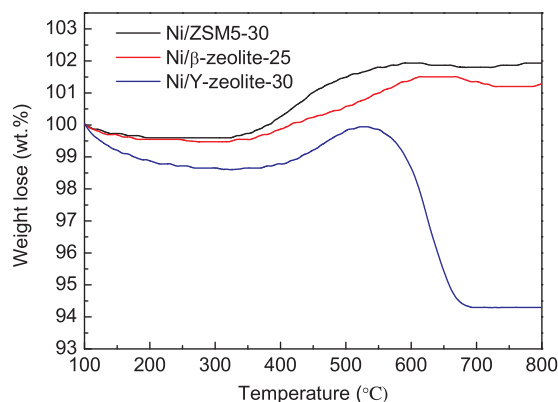|	Sand	ZSM5-30	β-zeolite-25	Y-zeolite-30	Ni/ZSM5-30	Ni/β-zeolite-25	Ni/Y-zeolite-30
H_2 yield, mmol H_2 $g_{plastic}^{-1}$	55.85	57.44	53.87	55.42	66.09	61.38	58.06
CO yield, mmol CO $g_{plastic}^{-1}$	31.30	31.80	29.59	31.73	34.63	33.54	32.19
Syngas yield, mmol $g_{plastic}^{-1}$	87.15	89.24	83.46	87.16	100.72	94.92	90.26
Gas yield in relation to plastic only, wt.%	144.40	146.50	133.54	144.20	165.59	157.59	160.52
Product Mass Balance, wt.%	102.94	101.33	97.31	97.61	103.07	103.07	103.31
Gas composition, vol.%							
H_2	54.43	54.99	55.58	53.99	56.20	55.84	53.64
CH_4	6.85	6.43	6.07	7.36	4.55	4.39	6.11
CO	30.50	30.45	30.53	30.92	29.45	30.51	29.74
CO_2	6.48	6.80	5.91	6.00	8.72	8.61	9.39
C_2-C_4	1.74	1.33	1.92	1.73	1.07	0.65	1.13

Fig. 7. Temperature programmed oxidation profiles of used Ni based catalysts with different support types (Ni/ZSM5-30, Ni/β-zeolite-25 and Ni/Y-zeolite-30).

oxidised to NiO during the TPO analysis. If it is assumed that all of the Ni in the spent catalyst was oxidized into NiO through TPO analysis, the calculated maximum increase in the catalyst mass would be ~2.73 wt. %, which was approximately the increase of catalyst mass revealed by the TPO results. This suggests that almost no coke was deposited on the used catalysts. The negligible carbon deposition for the all the used Ni supported ZSM5 catalysts with different Si:Al ratios, suggests that the two-stage pyrolysis-catalytic reforming process using the ZSM5 type catalysts was effective against catalyst coking.

All of the spent Ni/ZSM5 catalysts were further analysed by SEM, and typical SEM micrographs are shown in Fig. 10. Compared with the images in Fig. 2 for the fresh catalysts, there were no obvious differences between the fresh and spent catalysts in terms of structure and coke formation, except that just small quantities of filamentous carbon were found on the used Ni/ZSM5-50 catalyst. It has also been reported [33] that a Ni/ZSM5 catalyst showed a high resistance to coke formation, resulting in higher catalytic activity for hydrogen production from the catalytic steam reforming of polypropylene using Ni/ZSM5 compared with Ni/CeO₂, Ni/MgO and Ni/Al₂O₃ catalysts.

3.4. Investigation of process parameters for the Ni/ZSM5-30 catalyst

The Ni/ZSM5-30 catalyst generated the highest yield of hydrogen and carbon monoxide, therefore, further work was carried out to optimize the syngas product by changing the process parameters. The catalyst temperature of 650–850 °C was firstly investigated with and without catalyst for the pyrolysis-catalytic steam reforming of waste plastic. The results presented in Table 4 show that in the absence of a catalyst (with sand) the H_2 yield was significantly increased from 19.71 mmol $g_{plastic}^{-1}$ to 55.85 mmol $g_{plastic}^{-1}$ and CO yield increased from 4.04 to 31.30 mmol $g_{plastic}^{-1}$ when the temperature was increased from 650 to 850 °C. The introduction of the Ni/ZSM5-30 catalyst to the process further generated higher yields of gases. However, the effect of

catalyst temperature on the gas productions with Ni/ZSM5-30 was much less than the effect with sand only. The total syngas yield increased from 51.63 to 100.72 mmol $g_{plastic}^{-1}$ when the catalyst temperature was raised to 850 °C. It is suggested that both the thermal cracking reaction (R1) and reforming reaction (R2) of hydrocarbons were greatly enhanced by the increased temperature, due to the endothermic nature of the reactions. The decrease in C_{2+} gas concentrations further demonstrated the promoted reactions. The H_2 concentration remained at around 50–56 vol.%, and the CO concentration was increased and CO_2 reduced because of the reversed water gas shift reaction (R3) when the second stage reactor temperature was increased from 650 to 850 °C whether with catalyst or not. In addition, the amount of coke deposition on the reacted Ni/ZSM5-30 catalysts at different reaction temperatures was also determined from TPO analysis of the reacted Ni/ZSM5-30 catalysts, and the results are shown in Fig. 9. The production of coke at the lower temperature of 650 °C was 3.76 wt.% and then decreased to only 0.22 wt.% at 850 °C for the Ni/ZSM5-30 catalyst.

The influence of various steam feeding rates from 0 to 6 g h⁻¹ for the pyrolysis-catalytic steam reforming of waste plastic with the Ni/ZSM5-30 catalyst at a catalyst temperature of 850 °C are also shown in Table 4. The increase in the steam feeding rate sees a positive effect on the hydrogen production from the waste plastic. The H_2 yield was increased from 30.11 mmol $g_{plastic}^{-1}$ in the absence of steam to 66.09 mmol g_{platic}^{-1} at the steam feeding rate of 6 g h⁻¹. The CO yield was minimal without any steam because of the low oxygen content in the raw plastic sample (present due to contamination of the recycled HDPE), but increased markedly with input of steam. This was attributed to the reactions (R2) and (R3) taking place in the presence of steam. Correspondingly, Fig. 11 shows that the amount of coke deposition declined from 10.61 in the absence of steam to 0.22 wt.% when the steam feeding rate of 6 g h⁻¹ was used, because of the coke reforming reactions (R4) promoted by the increasing water, which also generated more CO and H_2. A similar trend was also found by Acomb at al. [34] when they increased the steam input from 0 to 4.74 g h⁻¹ for the pyrolysis-catalysis of waste polyethylene. They also suggested that both filamentous carbon and amorphous carbon were consumed with the introduction of steam. As for the volumetric gas composition, though hydrogen production was greatly promoted with more steam, the relative H_2 volumetric concentration in the product gas was decreased from 68.84 to 56.20 vol.% because of the increased production of CO in the product gases. The carbon conversion was also greatly enhanced from 0.21 to 0.78 wt.% when the steam feeding rate was increased from 0 to 6 g h⁻¹.

Comparison of the gas production with the different types of zeolite (Ni/ZSM5-30, Ni/β-zeolite-25 and Ni/Y-zeolite-30) shown in Table 2 and the influence of process parameters for the Ni/ZSM5-30 catalyst shown in Table 4, the changes in syngas yield under different temperatures and steam feeding rates were much more significant. Therefore, the reaction equilibrium of (R1)–(R4) contributed to the H_2 and CO production from waste plastics using the Ni/zeolite catalysts were
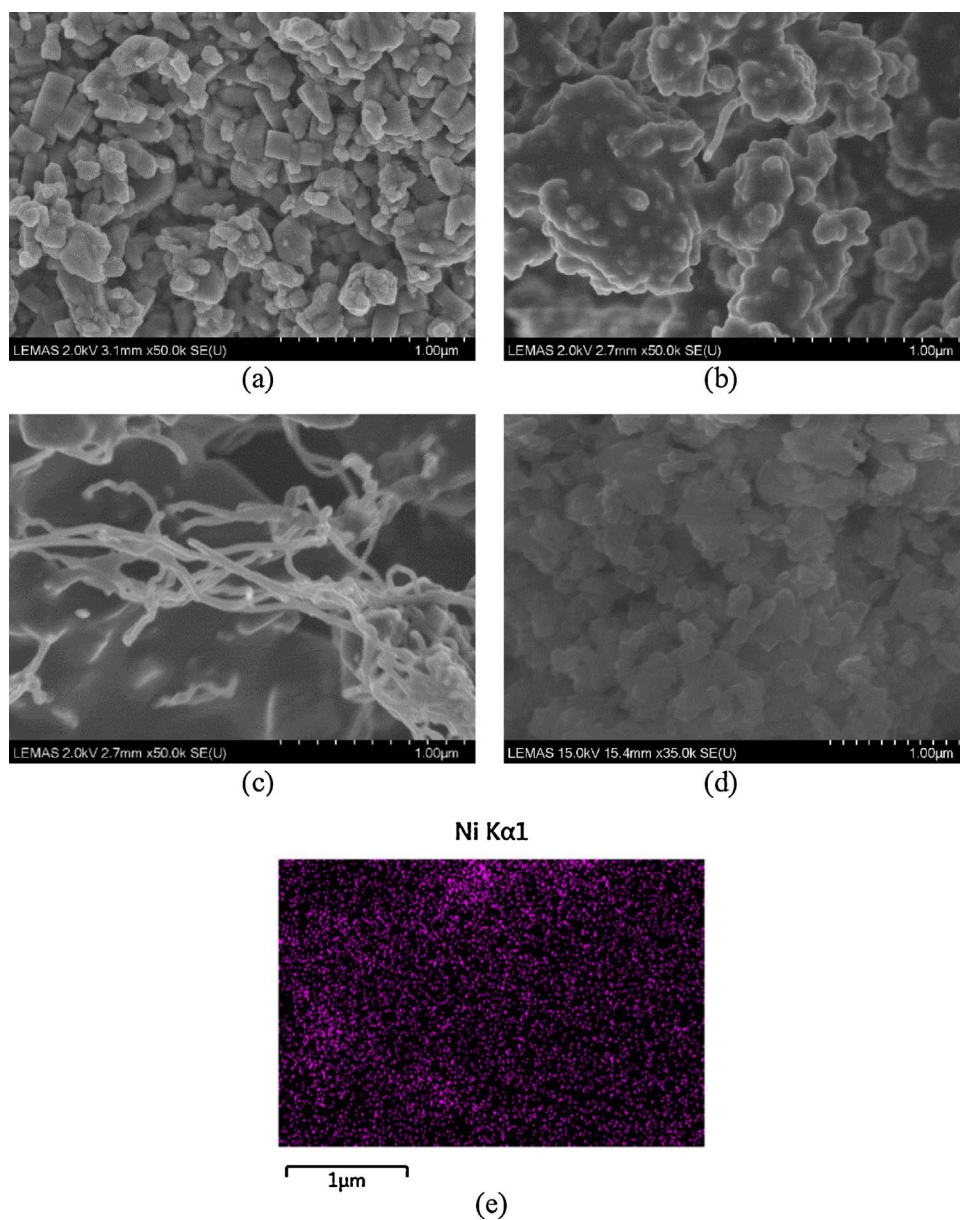
Fig. 8. SEM micrographs of used Ni based zeolites. (a) Ni/ZSM5-30, (b) Ni/β-zeolite-25, (c) Ni/Y-zeolite-30, (d) and (e) Ni EDX mapping of used Ni/ZSM5-30.

Table 3
Gas production from pyrolysis-catalytic steam reforming of waste polyethylene at 850 °C and steam feeding rate of 6 g/h, using Ni/ZSM5 with different silica to aluminium ratios.

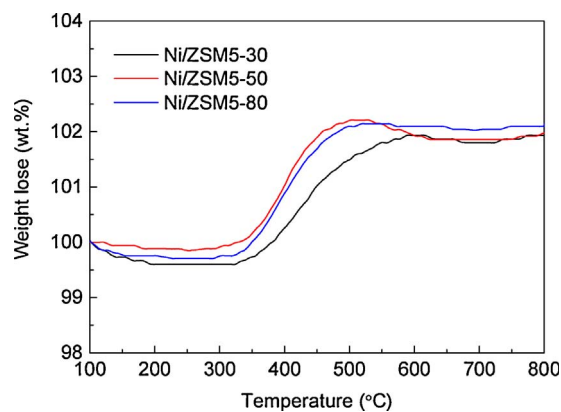|	Ni/ZSM5-30 (Si:Al ratio; 30)	Ni/ZSM5-50 (Si:Al ratio; 50)	Ni/ZSM5-80 (Si:Al ratio; 80)
H_2 yield, mmol g^{-1} plastic	66.09	60.55	59.87
CO yield, mmol g^{-1}	34.63	32.83	31.67
Syngas yield, mmol g^{-1}	100.72	93.37	91.54
Gas yield in relation to plastic only, wt.%	167.47	147.58	150.98
Mass Balance, %	103.07	100.65	101.24
Gas composition, vol.%			
H_2	56.20	57.02	56.24
CH_4	4.55	3.95	4.55
CO	29.45	30.91	29.75
CO_2	8.72	7.46	8.41
C_2-C_4	1.08	0.66	1.06

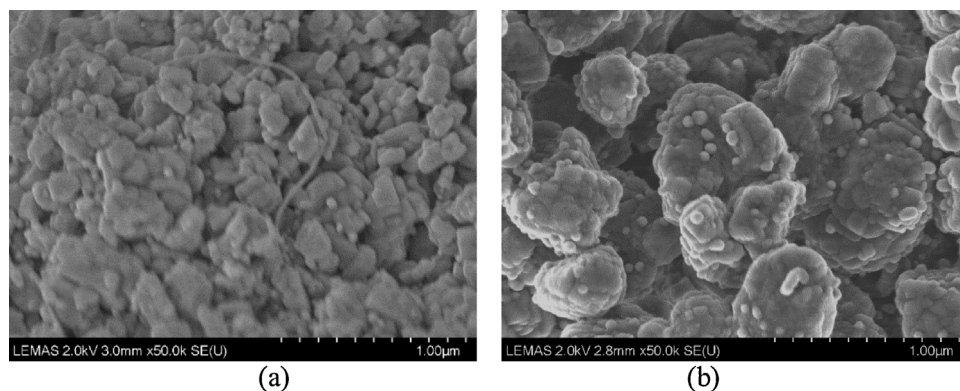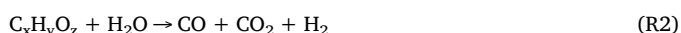**Fig. 9.** Temperature programmed oxidation profiles of the used Ni/ZSM5 catalysts in relation to Si:Al ratio.

dependent on the operational conditions such as temperature and steam feeding rate more than the dependence on the type of zeolite support. In addition, the coke formation was more serious under low catalytic temperature and low steam input because of the insufficient reforming reactions.

$$C_xH_yO_z \rightarrow CO + CO_2 + H_2 + CH_4 + H_2O + C_2 + \dots \quad (R1)$$

$$C_xH_yO_z + H_2O \rightarrow CO + CO_2 + H_2 \quad (R2)$$

$$CO + H_2O \rightarrow CO_2 + H_2 \quad (R3)$$

$$C + H_2O \rightarrow CO_2 + H_2 \quad (R4)$$
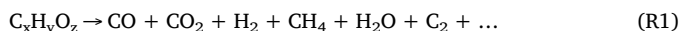
4. Conclusions

Ni/zeolite catalysts were investigated in relation to hydrogen and syngas production from the pyrolysis-catalytic steam reforming of waste high density polyethylene in a two stage reactor system.

(1) The catalyst activity of different zeolite type supported Ni based catalysts of hydrogen and syngas production was in the order of Ni/ZSM5-30 > Ni/β-zeolite-25 > Ni/Y-zeolite-30. Significant amounts of filamentous carbon (~6 wt.%) were observed on the reacted Ni/Y-zeolite-30 catalyst which accounted for the lower catalyst activity.
(2) The Ni/ZSM5 catalyst with a lower Si:Al ratio of 30 produced a higher syngas production of 100.72 mmol $g_{plastic}^{-1}$ compared with the Ni/ZSM5 catalysts with higher Si:Al ratios. In addition, ZSM5 was found to be effective for coke formation resistance as a support for
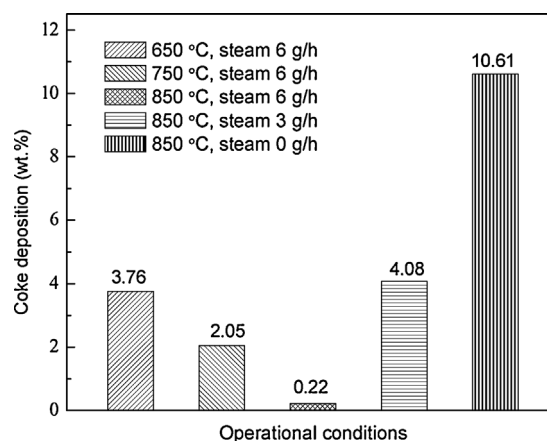

Fig. 11. The amount of coke deposition under different operational conditions for the Ni/ZSM5-30 catalyst.

Ni-based catalysts.
(3) The increase in catalyst temperature and steam feeding rate produced a positive effect on the syngas production from pyrolysis-catalytic steam reforming of waste high density polyethylene. An optimum operational condition was obtained at a catalyst temperature of 850 °C and steam feeding rate of 6 g h^{-1}.

Acknowledgements

Table 4

Gas production from pyrolysis-reforming of waste plastics at different conditional parameters at the presence of Ni/ZSM5-30.

	Process conditions							
Temperature, °C	650	750	850	650	750	850	850	850
Steam, g/h	6	6	6	6	6	6	3	0
Catalyst	sand	sand	sand	Ni/ZSM5-30	Ni/ZSM5-30	Ni/ZSM5-30	Ni/ZSM5-30	Ni/ZSM5-30
H$_2$ yield, mmol $g_{plastic}^{-1}$	19.71	42.51	55.85	43.02	65.02	66.09	62.09	30.11
CO yield, mmol $g_{plastic}^{-1}$	4.04	20.94	31.30	8.61	23.74	34.63	33.13	3.76
Syngas yield, mmol $g_{plastic}^{-1}$	23.75	63.46	87.15	51.63	88.76	100.72	95.22	33.87
Gas yield in relation to plastic only, wt.%	73.42	113.66	144.40	192.39	196.76	167.47	152.86	44.12
Mass Balance, %	102.28	101.41	102.94	106.02	106.36	103.54	100.62	99.12
Gas composition, vol.%								
H$_2$	49.41	56.28	54.43	47.53	54.91	56.20	56.18	68.84
CH$_4$	7.69	2.16	6.85	3.08	3.62	4.55	6.05	12.62
CO	10.13	27.72	30.50	9.51	20.04	29.45	29.98	8.60
CO$_2$	15.77	11.79	6.48	35.80	20.71	8.72	7.27	9.35
C$_2$-C$_4$	17.00	2.06	1.74	4.09	0.72	1.08	0.52	0.59
C conversion to gas, wt.%	0.45	0.52	0.72	0.75	0.77	0.78	0.73	0.21

References

[1] S. Sharma, S.K. Ghoshal, Renew. Sus. Energ. Rev. 43 (2015) 1151–1158.

[2] I. Dincer, C. Acar, Int. J. Hydrogen Energ. 40 (34) (2015) 11094–11111.

[3] R.X. Yang, L.R. Xu, S.L. Wu, K.H. Chuang, M.Y. Wey, Int. J. Hydrogen Energ. 42 (16) (2017) 11239–11251.

[4] PlasticsEurope, Plastics − The Facts 2015, (2015).

[5] C. Wu, P.T. Williams, Int. J. Hydrogen Energ. 34 (15) (2009) 6242–6252.

[6] C. Wu, P.T. Williams, Appl. Catal. B-Environ. 90 (1) (2009) 147–156.

[7] I. Barbarias, G. Lopez, J. Alvarez, M. Artetxe, A. Arregi, J. Bilbao, M. Olazar, Chem. Eng. J. 296 (2016) 191–198.

[8] B. Dou, K. Wang, B. Jiang, Y. Song, C. Zhang, H. Chen, Y. Xu, Int. J. Hdrogen Energ. 41 (6) (2016) 3803–3810.

[9] S. Czernik, R.J. French, Energ. Fuel. 20 (2) (2006) 754–758.

[10] T. Namioka, A. Saito, Y. Inoue, Y. Park, T.J. Min, S.A. Roh, K. Yoshikawa, Appl. Energ. 88 (6) (2011) 2019–2026.

[11] Y. Park, T. Namioka, S. Sakamoto, T.J. Min, S.A. Roh, K. Yoshikawa, Fuel Process. Technol. 91 (8) (2010) 951–957.

[12] S. De, J. Zhang, R. Luque, N. Yan, Energ. Environ. Sci. 9 (11) (2016) 3314–3347.

[13] C. Wu, P.T. Williams, Int. J. Hydrogen Energ. 35 (3) (2010) 949–957.

[14] A. Vizcaíno, A. Carrero, J. Calles, Int. J. Hydrogen Energ. 32 (10) (2007) 1450–1461.

[15] Y. Li, G. Lu, J. Ma, RSC Advs. 4 (34) (2014) 17420–17428.

[16] C. He, N. Zhao, Y. Han, J. Li, C. Shi, X. Du, Mat. Sci. Eng.-A 441 (1) (2006) 266–270.

[17] L.P. Teh, S. Triwahyono, A.A. Jalil, C.R. Mamat, S.M. Sadik, N.A.A. Fatah, R.R. Mukti, T. Shishido, RSC Adv. 5 (79) (2015) 64651–64660.

[18] W. Yao, J. Li, Y. Feng, X. Zhang, Q. Chen, S. Komarneni, Y. Wang, RSC Adv. 5 (39) (2015) 30485–30494.

[19] M.M. Yung, A.K. Starace, C. Mukarakate, A.M. Crow, M.A. Leshnov, K.A. Magrini, Energ. Fuel. 30 (7) (2016) 5259–5268.

[20] S. Karnjanakom, G. Guan, B. Asep, X. Du, X. Hao, C. Samart, A. Abudula, Energ. Convers. Manage. 98 (2015) 359–368.

[21] D. Yao, C. Wu, H. Yang, Y. Zhang, M.A. Nahil, Y. Chen, P.T. Williams, H. Chen, Energ. Convers. Manage. 148 (2017) 692–700.

[22] M.A. Nahil, C. Wu, P.T. Williams, Fuel Process. Technol. 130 (2015) 46–53.

[23] C. Muhammad, J.A. Onwudili, P.T. Williams, Energ. Fuel. 29 (4) (2015) 2601–2609.

[24] A. Veses, B. Puertolas, M.S. Callen, T. Garcia, Micropor. Mesopor. Mat. 209 (2015) 189–196.

[25] A. Akah, C. Colin, G. Arthur, Appl. Catal. B-Environ. 59 (3) (2005) 221–226.

[26] S. Wong, N. Ngadi, T.A.T. Abdullah, I.M. Inuwa, Ind. Eng. Chem. Res. 55 (9) (2016) 2543–2555.

[27] I.F. Elbaba, C. Wu, P.T. Williams, Int. J. Hydrogen Energ. 36 (11) (2011) 6628–6637.

[28] A. Ochoa, I. Barbarias, M. Artetxe, A.G. Gayubo, M. Olazar, J. Bilbao, P. Castaño, Appl. Catal. B-Environ. 209 (2017) 554–565.

[29] K. Jun, H.S. Lee, H.S. Roh, S.E. Park, Bull. Korean Chem. Soc. 24 (1) (2003) 106–108.

[30] X. Zhu, S. Liu, Y. Song, L. Xu, Appl. Catal. A-Gen. 288 (1) (2005) 134–142.

[31] D. Mores, E. Stavitski, M.H.F. Kox, J. Kornatowski, U. Olsbye, B.M. Weckhuvsen, Chem. Eur. J. 14 (36) (2008) 11320–11327.

[32] M. Guisnet, M.P. Magnoux, Catal. Today 36 (4) (1997) 477–483.

[33] C. Wu, P.T. Williams, Appl. Catal. B-Environ. 87 (3) (2009) 152–161.

[34] J.C. Acomb, C. Wu, P.T. Williams, Appl. Catal. B-Environ. 147 (2014) 571–584.